mum weight by 2.2%, making it the least restrictive constraint. The ply dropoff rate constraint increased the optimum weight by 6.3%. The ply percentage constraint increased the optimum weight by 17.3%, making it the most restrictive constraint. The combined effect of all three types of constraints was extremely restrictive, increasing the optimum weight by 35.3%.

Plies shifted from one zone to another when the constraints were applied individually. For example, when the ply dropoff rate constraint was applied, the plies from the thickest zone were reduced and the plies of adjacent thinner zones were increased. When the ply percentage constraint was applied, the plies were shifted from the 0-deg orientation to ± 45- and 90-deg orientations. An interleaving condition existed in the base run. When the ply interleaving constraint was applied, the − 45-deg plies in the thickest zone were increased to the level of − 45-deg plies in the adjacent thinner zones. When all three types of constraints were applied simultaneously, many plies were added and fewer were shifted in order to satisfy the constraints.

Acknowledgment

The authors would like to thank the Texas Higher Education Coordinating Board for sponsoring this research.

References

[1]Toakley, A. R., "Optimum Design Using Available Sections," *Journal of the Structural Division,* Vol. 94, No. ST5, 1968, pp. 1219-1241.

[2]Schmit, L. A., and Fleury, C., "Discrete-Continuous Variable Structural Synthesis Using Dual Methods," *AIAA Journal,* Vol. 18, No. 12, 1980, pp. 1515-1524.

[3]Jones, R. T., and Hague, D. S., "Application of Multivariable Search Techniques to Structural Design Optimization," NASA CR-2038, June 1972.

[4]Stroud, W. J., and Agranoff, N., "Minimum-Mass Design of Filamentary Composite Panels Under Combined Loads: Design Procedure Based On Simplified Buckling Equations," NASA TN D-8257, Oct. 1976.

[5]Petiau, C., "Structural Optimization of Aircraft," *Thin Walled Structures,* Vol. 11, 1991, pp. 43-64.

[6]Johnson, E. H., and Neill, D. J., "Automated Structural Optimization System 'ASTROS' Vol. 3—Applications Manual," Air Force Wright Aeronautical Labs., AFWAL-TR-88-3028, Wright-Patterson Air Force Base, OH, Dec. 1988.

[7]Wang, B. P., and Costin, D. P., "Optimum Design of a Composite Structure with Ply-Interleaving Constraints," *Third Air Force/NASA Symposium On Recent Advances in Multidisciplinary Analysis and Optimization,* Sept. 1990, pp. 553-561.

[8]Balinski, M. L., "Integer Programming: Methods, Uses, Computations," *Management Science,* Vol. 12, No. 3, 1965, pp. 253-313.

Composite Laminated Shells Under Internal Pressure

F. G. Yuan*
North Carolina State University, Raleigh, North Carolina 27695

Introduction

SHELLS of various constructions have been used extensively as load carrying structural components. With the unique characteristics of high strength/weight and stiffness/weight ratios in composite materials, composite laminated shells are receiving greater consideration for use in primary structures such as aircraft fuselages, solid rocket casings, submersibles, and space vehicles. One of the concerns in structural design is devoted to developing analytical methods for determining the response under various loading conditions. Sherrer[1] presented an elasticity solution for filament wound cylinders with axisymmetric loadings. Whitney and Halpin[2] have analyzed off-axis unidirectional two-layer angle-ply anisotropic tubes under various loading conditions based on Donnell's shallow shell approximations[3] to characterize the mechanical properties and behavior of fiber composites. Reuter[4] presented solutions for an alternate-ply cylindrical shell under internal pressure using Donnell's theory. The stress field of a single layer anisotropic cylinder due to mechanical loadings was considered by Pagano.[5] Hull et al.[6] studied failure mechanisms of a filament wound cylinder subjected to internal pressure. Hyer[7] has evaluated the stress distribution of cross-ply laminated shells under hydrostatic pressure.

This Note presents a theoretical study of the response of filament wound composite shells under internal pressure. Each layer of the material is generally cylindrically anisotropic. By using cylindrically anisotropic elasticity field equations and Lekhnitskii's stress functions, a system of sixth-order ordinary differential equations is obtained. The general expressions for the stresses and displacements in the laminated composite shells under internal pressure are discussed. Two composite systems, graphite/epoxy and glass/epoxy, are selected to demonstrate the influence of degree of material anisotropy and fiber orientations on the axial and induced twisting deformation. Stress distributions of $[45/-45]_s$ symmetric angle-ply fiber-reinforced laminated shells are shown to illustrate the effect of radius-to-thickness ratio.

Analysis

Consider a laminated cylindrical shell consisting of fiber-reinforced laminas subjected to internal pressure. It is assumed that the axis of anisotropy coincides with the longitudinal z axis. The shell is assumed to be long enough so that, in the region away from the ends, Saint Venant's principle holds. Consequently, the stress components are independent of the longitudinal z axis of the shell. As a result of axisymmetric deformation, one can establish a system of coupled governing ordinary differential equations in terms of Lekhnitskii's stress functions $F(r)$ and $\Psi(r)$[8,9] for the individual lamina:

$$L_4'F + L_3'\Psi = 0, \qquad L_3''F + L_2'\Psi = \frac{S_{34}A_3}{S_{33}r} - 2A_4 \tag{1}$$

where L_4', L_3', L_3'', and L_2' are linear ordinary differential operations defined as

$$L_4' = \tilde{S}_{22}\frac{d^4}{dr^4} + 2\tilde{S}_{22}\frac{1}{r}\frac{d^3}{dr^3} - \tilde{S}_{11}\frac{1}{r^2}\frac{d^2}{dr^2} + \tilde{S}_{11}\frac{1}{r^3}\frac{d}{dr}$$

$$L_3' = -\tilde{S}_{24}\frac{d^3}{dr^3} + (\tilde{S}_{14} - 2\tilde{S}_{24})\frac{1}{r}\frac{d^2}{dr^2}$$

$$L_3'' = -\tilde{S}_{24}\frac{d^3}{dr^3} - (\tilde{S}_{14} + \tilde{S}_{24})\frac{1}{r}\frac{d^2}{dr^2}$$

$$L_2' = \tilde{S}_{44}\frac{d^2}{dr^2} + \tilde{S}_{44}\frac{1}{r}\frac{d}{dr} \tag{2}$$

where A_3 and A_4 pertain to uniform axial deformation and relative angle of rotation about the z axis. The reduced compliance constants $\tilde{S}_{ij}$ are defined as

$$\tilde{S}_{ij} = S_{ij} - \frac{S_{i3}S_{j3}}{S_{33}} \qquad (i,j = 1,2,4,5,6)$$

Received March 19, 1991; revision received Sept. 18, 1991; accepted for publication Sept. 23, 1991.

*Assistant Professor, Department of Mechanical and Aerospace Engineering. Member AIAA.

The stress components in terms of the stress functions may be expressed as

$$\sigma_r = \frac{1}{r}\frac{dF}{dr}, \quad \sigma_\theta = \frac{d^2F}{dr^2}, \quad \tau_{\theta z} = -\frac{d\Psi}{dr}$$

$$\sigma_z = (A_3 - S_{13}\sigma_r - S_{23}\sigma_\theta - S_{34}\tau_{\theta z})/S_{33} \tag{3}$$

The displacements have the following form:

$$u_r = U_r(r) + u_r^0, \qquad u_\theta = A_4 rz + U_\theta(r) + u_\theta^0,$$

$$w = A_3 z + W(r) + w^0 \tag{4}$$

The U_r, U_θ, and W represent the pure deformation field, and the u_r^0, u_θ^0, and w^0 characterize rigid-body displacements.

The solution of the coupled differential equations (1) can be expressed as

$$F(r) = a_1 r^3 + a_2 r^2 + C_0 r + \sum_{k=1}^{2} C_k\, r^{1+\mu_k} \tag{5}$$

$$\Psi(r) = b_1 r^2 + b_2 r + C_0\eta_0 \ell n\, r + \sum_{k=1}^{2} C_k\, \eta_k r^{\mu_k} \tag{6}$$

$$\tau_{\theta z} = -\kappa_3 A_3 - \kappa_4 A_4 r - \sum_{k=1}^{2} C_k \eta_k \mu_k r^{\mu_k - 1} \tag{8}$$

$$\sigma_z = [1 - (S_{13} + S_{23})\kappa_1 + S_{34}\kappa_3]\frac{A_3}{S_{33}} - [(S_{13} + 2S_{23})\kappa_2 - S_{34}\kappa_4]\frac{A_4 r}{S_{33}} - \sum_{k=1}^{2} C_k[S_{13}(1+\mu_k) + S_{23}(1+\mu_k)\mu_k - S_{34}\eta_k\mu_k]\frac{r^{\mu_k - 1}}{S_{33}}$$

The displacements excluding the rigid-body displacements are expressed as

$$u_r = D_1 A_3 r + D_2 A_4 r^2 + \sum_{k=1}^{2} C_k[\tilde{S}_{11}(1+\mu_k)/\mu_k + \tilde{S}_{12}(1+\mu_k) - \tilde{S}_{14}\eta_k]r^{\mu_k} \tag{9}$$

$$u_\theta = A_4 rz, \qquad w = A_3 z$$

where

$$D_1 = \frac{(\tilde{S}_{11} + \tilde{S}_{12})[S_{34}\tilde{S}_{24} + (S_{13} - S_{23})\tilde{S}_{44}] - \tilde{S}_{14}[S_{34}(\tilde{S}_{12} + \tilde{S}_{22}) + (S_{13} - S_{23})(\tilde{S}_{14} + \tilde{S}_{24})]}{[(\tilde{S}_{14}^2 - \tilde{S}_{24}^2) - (\tilde{S}_{11} - \tilde{S}_{22})\tilde{S}_{44}]S_{33}} + \frac{S_{13}}{S_{33}}$$

$$D_2 = [(\tilde{S}_{11} + 2\tilde{S}_{12})\tilde{S}_{24} - (\tilde{S}_{12} + 2\tilde{S}_{22})\tilde{S}_{14}]/[(\tilde{S}_{11} - 4\tilde{S}_{22})\tilde{S}_{44} - (\tilde{S}_{14}^2 - 4\tilde{S}_{24}^2)]$$

where

$$\eta_0 = \frac{\tilde{S}_{11}}{\tilde{S}_{14}}, \quad \eta_k = \frac{\tilde{S}_{14} + \tilde{S}_{24}\mu_k}{\tilde{S}_{44}}\frac{1+\mu_k}{\mu_k}, \quad (k = 1,2)$$

$$\mu_{1,2} = \pm\left(\frac{\tilde{S}_{11}\tilde{S}_{44} - \tilde{S}_{14}^2}{\tilde{S}_{22}\tilde{S}_{44} - \tilde{S}_{24}^2}\right)^{1/2}$$

and C_1 and C_2 are unknown constants to be determined later. Note that the μ_k are real due to the positive definiteness of $\tilde{S}_{ij}$. The remaining constants are obtained by substituting Eqs. (5) and (6) into Eq. (1) and then using the displacement field to be continuous and single-valued.

$$C_0 = 0$$

$$3a_1 = (2\tilde{S}_{24} - \tilde{S}_{14})A_4/[(\tilde{S}_{11} - 4\tilde{S}_{22})\tilde{S}_{44} - (\tilde{S}_{14}^2 - 4\tilde{S}_{24}^2)] \equiv \kappa_2 A_4$$

$$2b_1 = (4\tilde{S}_{22} - \tilde{S}_{11})A_4/[(\tilde{S}_{11} - 4\tilde{S}_{22})\tilde{S}_{44} - (\tilde{S}_{14}^2 - 4\tilde{S}_{24}^2)] \equiv \kappa_4 A_4$$

$$2a_2 = [S_{34}(\tilde{S}_{24} - \tilde{S}_{14}) - \tilde{S}_{44}(S_{23} - S_{13})]A_3/[(\tilde{S}_{14}^2 - \tilde{S}_{24}^2) - (\tilde{S}_{11} - \tilde{S}_{22})\tilde{S}_{44}]S_{33} \equiv \kappa_1 A_3$$

$$b_2 = [(S_{13} - S_{23})(\tilde{S}_{14} + \tilde{S}_{24}) + (\tilde{S}_{22} - \tilde{S}_{11})S_{34}]A_3/[(\tilde{S}_{14}^2 - \tilde{S}_{24}^2) - (\tilde{S}_{11} - \tilde{S}_{22})\tilde{S}_{44}]S_{33} \equiv \kappa_3 A_3 \tag{7}$$

The final expressions for the stresses are

$$\sigma_r = \kappa_1 A_3 + \kappa_2 A_4 r + \sum_{k=1}^{2} C_k(1+\mu_k)r^{\mu_k - 1}$$

$$\sigma_\theta = \kappa_1 A_3 + 2\kappa_2 A_4 r + \sum_{k=1}^{2} C_k(1+\mu_k)\mu_k r^{\mu_k - 1}$$

Assuming that the bond between the laminae is perfect, the continuity conditions of the stress and displacement along the interface between the kth and $(k+1)$th lamina are given by

$$\sigma_r^{(k)} = \sigma_r^{(k+1)}, \qquad u_r^{(k)} = u_r^{(k+1)} \tag{10}$$

$$A_3^{(k)} = +A_3^{(k+1)}, \qquad A_4^{(k)} = A_4^{(k+1)} \tag{11}$$

The applied loadings at the ends of the composite shell are replaced by the following equivalent resultant forces and moments

$$\int_A \sigma_z r\, dr\, d\theta = P_z, \qquad \int_A \tau_{\theta z} r^2\, dr\, d\theta = 0 \tag{12}$$

where P_z is the applied axial load resulting from the internal pressure acting on the enclosure of the end cross sections with area A. For an N layer laminated cylindrical shell with $2N$ unknown constants and A_3 and A_4 under consideration, these constants can be determined by imposing $2(N-1)$ interfacial displacement and traction continuity conditions, Eqs. (12), and two traction boundary conditions at the inner and outer cylindrical surfaces.

Results and Discussions

The method developed in the preceding section is implemented for studying cylindrical composite laminated shells with end closures under internal pressure. The axial load exerted by the internal pressure on the ends of the cross section can be simulated as $P_z = \pi(R - h/2)^2 p_i$, where p_i is the magnitude of the internal pressure, and R and h are midradius and thickness of the shell, respectively. Graphite/epoxy and glass/epoxy composite materials with high and low material anisotropy are used for numerical calculations and their material properties are used as follows: graphite/epoxy—$E_L = 172.375$ GPa, $E_T = E_Z = 6.895$ GPa, $G_{LT} = G_{LZ} = 3.448$ GPa, $G_{TZ} = 1.379$ GPa, $\nu_{LT} = \nu_{LZ} = \nu_{TZ} = 0.25$; glass/epoxy—$E_L = 41.37$ GPa, $E_T = E_Z = 13.79$ GPa, $G_{LT} = G_{LZ} = 5.516$ GPa, $G_{TZ} = 2.758$ GPa, $\nu_{LT} = \nu_{LZ} = \nu_{TZ} = 0.25$, where L, T, and Z refer to material principal axes along fiber, transverse, and thick-

ness directions, respectively. The lamination angle α is measured in the counterclockwise direction from the longitudinal direction of the shell. The stacking sequence is ordered starting from the outer layer of the shell.

To gain insight into the effects of curvilinear material anisotropy, fiber orientation, and stacking sequence, the axial and induced twisting deformation under internal pressure will be first studied in detail. For the case of composite shells with various values of off-angle α, Fig. 1a illustrates the extensional and twisting deformation of graphite/epoxy and glass/epoxy composites for midradius-to-thickness ratio $S = R/h = 10$. The extensional deformation for graphite/epoxy remains almost the same value in the region $0 \leq \alpha \leq 15$ deg and then increases monotonically. However, for glass/epoxy, the

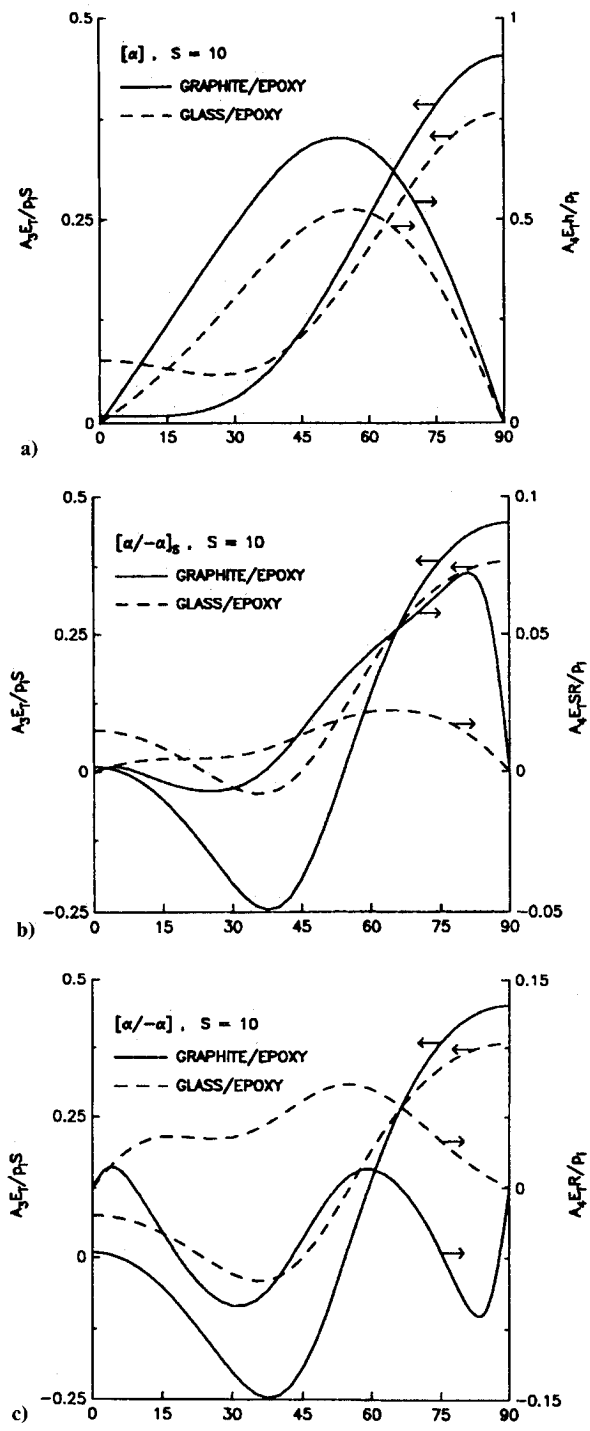

Fig. 1 Axial and induced twisting deformation of a composite cylindrical shell.

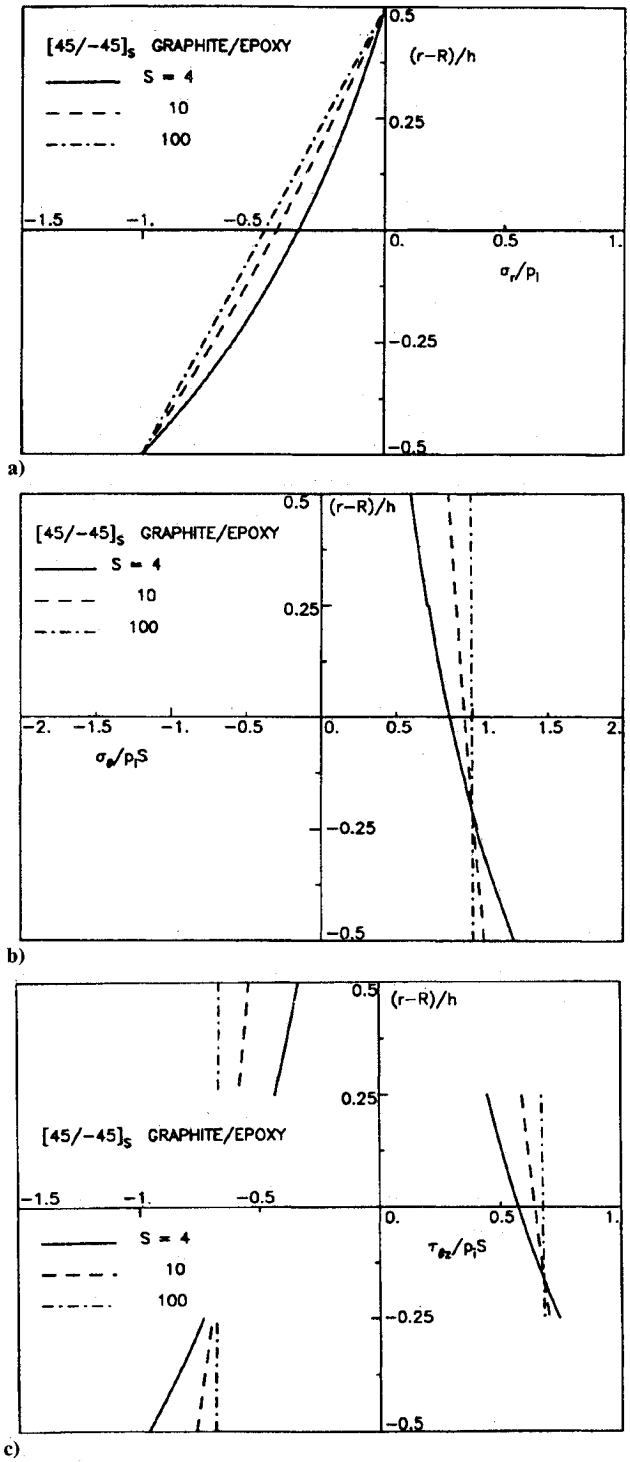

Fig. 2 Distribution of stresses through the thickness direction in a $[45/-45]_s$ graphite/epoxy composite shell.

deformation decreases in the region from 0 to 26 deg and then increases. A relatively large induced twisting deformation of the off-axis undirectional graphite/epoxy composite shell prevails due to strong material anisotropy. The twisting deformation reaches maximum values at $\alpha \simeq 52$ and 57 deg for graphite/epoxy and glass/epoxy, respectively. The deformation behaviors of $[\pm\alpha]_s$ layup for these two composite systems are demonstrated in Fig. 1b. A wide range $5 \leq \alpha \leq 53$ deg of shortening deformation due to Poisson effect for graphite/epoxy under internal pressure can be seen in the figure. For low anisotropy of the glass/epoxy material, a smaller range of shortening deformation $24 \leq \alpha \leq 45$ deg is observed. The twisting deformation is relatively small due to the symmetric layup. Reversal of induced twisting deformation occurs from

$\alpha = 9.5$–36 deg for graphite/epoxy shown in Fig. 1b. The figure also shows that the twisting deformation of graphite epoxy has highest value at $\alpha \simeq 82.5$ deg and has a steep gradient as the angle approaches 90 deg. However, no reversal of twisting deformation for glass/epoxy is found. Figure 1c illustrates the axial and induced twisting deformation for $[\alpha/-\alpha]$ unsymmetric laminated shell of graphite/epoxy and glass/epoxy composites. Because of the nature of the layup, the shells exhibit coupling between stretching and twisting. Since the extensional stiffness is one order of magnitude higher than the coupling stiffness, variations of axial deformation with fiber orientation shown in Fig. 1c have almost the same curves as those of $[\alpha/-\alpha]_s$. Reversal of twisting deformation occurs in most of the angles studied for graphite/epoxy, and there is no reversal of twisting deformation for glass/epoxy.

The $[45/-45]_s$ angle-ply composite laminated shell is selected here as another example because of technical importance. The σ_r distribution through the thickness for three values of S is illustrated in Fig. 2a. As the S increases, the distribution tends to vary linearly through the thickness direction. Figures 2b and 2c depict the distributions of in-plane stresses σ_θ and $\tau_{\theta z}$ through the thickness. A slight discontinuity of σ_θ across the $45/-45$ interface is shown in Fig. 2b. As the shell becomes thinner, the σ_θ approaches a uniform distribution through the thickness and is in agreement with the results obtained from simple strength of materials approach and a stress ratio of 2:1 results for σ_θ vs σ_z. It is found in Fig. 2c that $\tau_{\theta z}$ has the same order of magnitude as σ_θ. The distribution changes significantly with the thickness direction and alters its sign across the interface. It is also noted from the figure that the inner layer of the shell is stressed more than the outer layer for thick shells under internal pressure.

Summary and Conclusions

An analytical study of the deformation and stress response in laminated cylindrical shells under internal pressure has been presented. Formulations of the problem are based on cylindrically anisotropic elasticity equations with the aid of Lekhnitskii's stress functions. In general, stress components σ_r, σ_θ, σ_z, and $\tau_{\theta z}$ and accompanying axial and twisting deformations will all be present in the composite shells subjected to internal pressure. Two composite systems, graphite/epoxy and glass/epoxy, are selected to demonstrate the influence of material anisotropy and fiber orientations on the axial and twisting deformation. As is expected, materials with low anisotropy usually have small induced twisting deformation. Depending on the fiber orientations, the shell may experience shortening axial deformation or reversed twisting deformation under internal pressure. Even for $[\pm\alpha]_s$ off-axis angle-ply laminated shells, the structure experiences small degree of twisting deformation due to the radial variation of the material distribution. Stress distributions of symmetric $[45/-45]_s$ graphite/epoxy composite shells have been examined in detail. For the case studied, for very thin shells, the interlaminar normal stress distribution exhibits linear variation through the thickness and the in-plane stresses can be modeled from simple strength-of-material approach.

Acknowledgments

This research is supported by NASA Grant NAGW-1331 to the Mars Mission Research Center. Special thanks to K. Choi who drew the figures.

References

[1]Sherrer, R. E., "Filament-Wound Cylinders with Axial-Symmetric Loads," *Journal of Composite Materials*, Vol. 1, No. 4, 1967, pp. 344–355.

[2]Whitney, J. M., and Halpin, J. C., "Analysis of Laminated Anisotropic Tubes Under Combined Loadings," *Journal of Composite Materials*, Vol. 2, No. 3, 1968, pp. 360–367.

[3]Donnell, L. H., "Stability of Thin-Walled Tubes under Torsion," NACA Rept. 479, 1933.

[4]Reuter, R. C., Jr., "Analysis of Shells Under Internal Pressure," *Journal of Composite Materials*, Vol. 6, Jan. 1972, pp. 94–113.

[5]Pagano, N. J., "The Stress Field in a Cylindrically Anisotropic Body Under Two-Dimensional Surface Tractions," *ASME Journal of Applied Mechanics*, Vol. 39, No. 9, 1972, pp. 791–796.

[6]Hull, D., Legg, M. J., and Spencer, B., "Failure of Glass/Polyester Filament Wound Pipe," *Composites*, Vol. 9, No. 1, 1978, pp. 17–24.

[7]Hyer, M. W., "Hydrostatic Response of Thick Laminated Composite Cylinders," *Journal of Reinforced Plastics and Composites*, Vol. 7, July 1988, pp. 321–340.

[8]Lekhnitskii, S. G., *Theory of Elasticity of an Anisotropic Elastic Body*, Holden-Day, San Francisco, CA, 1963.

[9]Yuan, F. G., "Exact Solutions for Laminated Composite Cylindrical Shells in Cylindrical Bending," *Journal of Reinforced Plastics and Composites*, Vol. 11, No. 4, 1992, pp. 340–371.